

Decoupled Conformal Optimisation: Efficient Prediction Sets via Independent Tuning and Calibration

Fanyi Wu^{1,2} Lihua Niu¹ Samuel Kaski^{1,3,4} Michele Caprio¹

¹Department of Computer Science, University of Manchester, Manchester, UK

²UKRI AI Centre for Doctoral Training in Decision Making for Complex Systems

³Department of Computer Science, Aalto University, Espoo, Finland

⁴ELLIS Institute, Finland

Correspondence: `fanyi.wu@manchester.ac.uk`

Abstract

Bayesian conformal optimisation methods often use the same held-out data both to search for efficient prediction sets and to certify coverage or risk. This coupling is natural for high-probability risk-control guarantees, but it is not necessary when the target is standard finite-sample marginal conformal coverage. We propose Decoupled Conformal Optimisation (DCO), a train-tune-calibrate design principle that uses an independent tuning split for efficiency-oriented structural selection and a fresh calibration split for the final conformal quantile. Conditional on the tuned structure, standard split-conformal exchangeability yields finite-sample marginal coverage for any candidate class, without a confidence parameter or multiple-testing correction. DCO therefore targets a different finite-sample guarantee from PAC-style methods: marginal conformal coverage rather than high-probability risk control. Under consistency assumptions on the coupled risk bound, the two approaches nevertheless converge to the same population threshold. Across classification and regression benchmarks, including ImageNet-A, CIFAR-100, Diabetes, California Housing, and Concrete, DCO tracks the nominal coverage level closely while often reducing average prediction-set size or interval width relative to PAC-style calibration. On ImageNet-A, for example, the average set size decreases from 26.52 to 25.26 and the 95th-percentile set size from 58.95 to 53.73; on Diabetes, the average interval width decreases from 2.098 to 1.914.

1 Introduction

Reliable uncertainty quantification is a central goal in modern machine learning. Conformal prediction (CP) offers a distribution-free way to construct prediction sets with finite-sample marginal coverage under exchangeability (Vovk et al., 2005; Shafer and Vovk, 2008; Angelopoulos and Bates, 2022; Barber et al., 2023; Caprio, 2025). In split CP, the data are divided into separate roles. A model is fitted on D_{train} . A non-conformity score $S(x, y)$ is then evaluated on an independent calibration set D_{cal} . The prediction set is

$$C(x) = \{y : S(x, y) \leq \hat{q}_{1-\alpha}\}, \quad (1)$$

where $\hat{q}_{1-\alpha}$ is the empirical $(1 - \alpha)$ conformal quantile of the calibration scores. The final threshold in (1) is an order statistic. Once the score and model structure have been fixed, this order statistic is computed on calibration data that are independent of the test point. This is the structural condition behind the standard exchangeability proof and the resulting finite-sample marginal coverage guarantee; see Appendix A.

Modern conformal methods increasingly seek more than validity. They also aim for efficiency: prediction sets should be small, informative, and still valid. In conformal optimisation, efficiency can be improved through the score, the prior, the surrogate model, or the threshold-search rule (Caprio et al., 2024, 2025). These choices introduce a simple but important design question: **which data should be used for optimisation, and which data should be reserved for calibration?**

The question matters because the two roles are statistically different. Optimisation searches for an efficient prediction rule. Calibration certifies the final rule by computing a conformal quantile. If the same held-out split is used for both roles, the final threshold is no longer computed on data untouched by the preceding search. The usual split-conformal exchangeability argument therefore does not apply directly. The problem is not optimisation itself. It is the reuse of the calibration data for both search and certification.

This distinction is particularly relevant for coupled risk-control procedures, including Conformal Risk Control (CRC) and PAC-style calibration based on Bayesian quadrature (BQ) (Angelopoulos et al., 2025b; Snell and Griffiths, 2025). Such methods select a threshold that satisfies a risk constraint with confidence $1 - \delta$. The coverage guarantees derived from PAC-style methods are different from the marginal coverage guarantee of split CP. PAC-style methods like CRC and BQ calibration target high-probability risk control, whereas split CP targets marginal coverage at level $1 - \alpha$. When marginal conformal coverage is the desired guarantee, it is natural to ask whether optimisation and calibration need to be coupled on the same data.

We answer this question with *Decoupled Conformal Optimisation* (DCO). DCO-Warmstart is a train-tune-calibrate design principle for Bayesian conformal optimisation. It assigns each data split a distinct role. The training split fits the Bayesian model. The tuning split D_{tune} selects efficiency-oriented structure, such as the score, prior, model configuration, or threshold-search rule. The calibration split D_{cal} is used only after this selection step. Its sole purpose is to compute the final conformal quantile.

This separation restores the split-conformal logic. Conditional on the structure selected using D_{train} and D_{tune} , the calibration scores and the test score remain exchangeable. The final threshold is then an order statistic of an untouched calibration set. Hence the standard split-conformal proof applies without modification, yielding finite-sample marginal coverage; see Appendix B. At the same time, DCO-Warmstart still allows explicit optimisation before calibration.

The idea is close in spirit to selecting a model on a validation set before applying split CP. The validity argument is the classical one. The contribution is to make the data-separation principle explicit for Bayesian conformal optimisation pipelines, where efficiency search and coverage assessment are often intertwined. It also clarifies the guarantee being targeted: marginal conformal coverage rather than high-probability risk control.

Our contributions are as follows:

- **A decoupled train-tune calibrate principle.** We formulate DCO-Warmstart as a simple design principle for Bayesian conformal optimisation. Structural choices are selected on D_{tune} , while the final conformal quantile is computed on an untouched D_{cal} .
- **A finite-sample marginal coverage guarantee.** We show that DCO-Warmstart inherits the standard split-conformal coverage guarantee once the tuned structure is fixed independently of D_{cal} . No confidence parameter δ is needed. No multiple-testing correction over the candidate class is required for the final conformal calibration.
- **A comparison with CRC/BQ-style calibration.** We clarify the difference between the finite-sample guarantees of DCO-Warmstart and CRC/BQ-style methods. DCO-Warmstart targets marginal conformal coverage. CRC/BQ-style methods target high-probability risk control. We also show that, under uniform consistency conditions on the risk estimator, both

approaches converge to the same population threshold,

$$\lambda^* = \inf\{\lambda : R(\lambda) \leq \alpha\}. \tag{2}$$

- **Empirical evidence across regression and classification.** We evaluate DCO-Warmstart on ImageNet-A, CIFAR-100, Diabetes, California Housing, and Concrete, with additional ablations over candidate search, split allocation, and target coverage level. Across these settings, DCO-Warmstart tracks nominal coverage closely and often reduces average set size or interval width relative to BQ/CRC-style calibration.

2 Related Work

We organise related work around a central distinction: whether optimisation and calibration are performed jointly on the same held-out data, or separated across independent splits. This perspective organises classical CP, score-design methods, BCP-CRC, LTT, ROCP, and DCO-Warmstart along a common dimension: how optimisation and calibration data are allocated. It also clarifies the statistical role played by each data split.

Quantile-based calibration. Classical CP (Vovk et al., 2005; Shafer and Vovk, 2008) provides distribution-free finite-sample coverage by setting the threshold to an empirical quantile of non-conformity scores, without explicit threshold optimisation. Efficiency is therefore largely governed by the non-conformity score (Bellotti, 2021; Dhillon et al., 2024; Sadinle et al., 2018). A substantial literature improves efficiency by reshaping the score rather than the final conformal threshold. Examples include adaptive classification scores such as RAPS (Angelopoulos et al., 2021), regression-adapted residuals (Lei et al., 2018), and posterior predictive densities via AOI importance reweighting in Bayesian settings (Fong and Holmes, 2021). Since score design and conformal quantile calibration play distinct statistical roles, DCO-Warmstart is compatible with scores from this line of work.

Risk-constrained threshold optimisation. A second line of work treats the threshold λ as a decision variable. BCP-CRC (Wu et al., 2026), for example, selects λ by minimising expected prediction set size subject to a high-probability miscoverage constraint enforced through the L^+ bound of CRC (Angelopoulos et al., 2025b; Snell and Griffiths, 2025):

$$\begin{aligned} \min_{\lambda} \quad & \mathbb{E}_X[|C(X; \lambda)|] \\ \text{s.t.} \quad & \mathbb{P}(\mathbb{P}(Y \notin C(X; \lambda)) \leq \alpha) \geq 1 - \delta. \end{aligned} \tag{3}$$

Here the inner probability is the population miscoverage risk for a fixed threshold, while the outer probability is taken over the draw of the calibration sample. Thus, (3) gives a high-probability risk-control statement over the calibration sample, rather than the standard marginal coverage guarantee of split CP (Vovk et al., 2005; Shafer and Vovk, 2008). Such a guarantee is useful when the objective is risk certification, especially with limited calibration data or frequent recalibration. The trade-off is that threshold selection and risk certification are performed on the same held-out data, making BCP-CRC the closest coupled baseline to DCO-Warmstart.

DCO-Warmstart is not a replacement for CRC/BQ-style methods when the scientific objective is high-probability risk control. The procedures target different statistical guarantees. CRC/BQ-style methods are appropriate when one wants a risk certificate that holds with confidence $1 - \delta$ over the calibration sample. DCO-Warmstart is appropriate when the target guarantee is the standard finite-sample marginal coverage guarantee of split CP. Our claim is therefore not that coupled

Table 1: Comparison of optimisation and calibration roles across methods. For methods with a confidence parameter, δ denotes the failure probability; the guarantee holds with confidence $1 - \delta$ over the calibration sample.

Method	Optimisation data	Calibration data	Guarantee	Confidence parameter
Split CP	none / fixed score	D_{cal}	Marginal coverage	No
Score-tuned CP	D_{tune}	D_{cal}	Marginal coverage	No
CRC/BQ-style	D_{cal}	D_{cal}	High-probability risk control	Yes, δ
LTT	D_{val} (via testing)	same as optimisation	High-probability risk control	Yes, δ
ROCP	D_{opt}	D_{cal}	Marginal coverage	No
DCO-Warmstart	D_{tune}	D_{cal}	Marginal coverage	No
DirectTune	D_{tune}	none	None in general	No

calibration is unnecessary in general, but that it is unnecessary for marginal conformal coverage when optimisation can be performed on an independent tuning split.

Learn-then-Test (LTT) (Angelopoulos et al., 2025a) also operates in a population-risk regime, but calibrates feasibility through hypothesis testing rather than constrained optimisation. Like CRC/BQ-style methods, it targets high-probability risk control rather than marginal split-conformal coverage.

Decision-theoretic set optimisation. Risk-Optimal Conformal Prediction (ROCP) (Wang and Dobriban, 2026) optimises the full prediction-set construction and downstream action rules for decision quality, and then applies CP on independent data to restore marginal coverage. Like DCO-Warmstart, ROCP separates the optimisation stage from the final conformal calibration step. The difference is scope: ROCP intervenes at the level of the entire set-construction and action rule, whereas DCO-Warmstart intervenes at the level of Bayesian structural and threshold-search configuration.

Where DCO-Warmstart fits. The methods above differ along two dimensions: what is optimised and when certification occurs. Classical CP certifies directly by an empirical quantile without threshold optimisation. Score-design methods optimise the score before calibration and then certify by quantile. BCP-CRC and related CRC/BQ-style methods optimise and certify risk on the same held-out data. LTT certifies population-risk feasibility through testing. ROCP optimises set structure and then calibrates on independent data.

DCO-Warmstart occupies a complementary position. Structural choices are selected on an independent tuning split, while the final conformal quantile is computed on a separate calibration split. This recovers the standard finite-sample marginal coverage guarantee without an additional confidence parameter. At the same time, under consistency assumptions on the coupled risk bound, DCO-Warmstart remains asymptotically aligned with CRC/BQ-style methods at the level of the population threshold. This asymptotic alignment should not be interpreted as an equivalence of finite-sample guarantees: DCO-Warmstart targets marginal coverage, whereas CRC/BQ-style methods target high-probability risk control. The practical consequence is a difference in finite-sample guarantee type, which we examine empirically in Section 5.

3 Theoretical Background

We formalise the prediction problem and establish the theoretical properties of DCO-Warmstart. All proofs are deferred to Appendix B.

3.1 Problem Setup

Let $(X, Y) \in \mathcal{X} \times \mathcal{Y}$ be drawn i.i.d. from an unknown distribution P . Prediction sets are parameterised by structural choices $\phi \in \Phi$, such as the score function type, prior hyperparameters, or model architecture, together with a scalar threshold $\lambda \in \Lambda$:

$$C_{\phi, \lambda}(x) = \{y : S_{\phi}(x, y) \leq \lambda\}, \quad (4)$$

where S_{ϕ} is a non-conformity score derived from the posterior predictive distribution $p(y | x, D_{\text{train}})$. Larger λ produces larger prediction sets; we assume $\lambda_1 \leq \lambda_2$ implies $C_{\phi, \lambda_1}(x) \subseteq C_{\phi, \lambda_2}(x)$. The two quantities of interest are the population miscoverage risk and expected set size,

$$R(\phi, \lambda) = \mathbb{P}(Y \notin C_{\phi, \lambda}(X)), \quad \mathcal{S}(\phi, \lambda) = \mathbb{E}[|C_{\phi, \lambda}(X)|], \quad (5)$$

and the data are partitioned into three independent splits: D_{train} for model fitting, D_{tune} for structural optimisation, and D_{cal} for conformal calibration.

3.2 Finite-sample marginal coverage of DCO-Warmstart

DCO-Warmstart selects structural choices on D_{tune} by solving the empirical problem

$$(\hat{\phi}_{\text{tune}}, \hat{\lambda}_{\text{tune}}) \in \arg \min_{(\phi, \lambda) \in \Phi \times \Lambda} \hat{\mathcal{S}}_{\text{tune}}(\phi, \lambda) \quad \text{s.t.} \quad \hat{R}_{\text{tune}}(\phi, \lambda) \leq \alpha, \quad (6)$$

where \hat{R}_{tune} and $\hat{\mathcal{S}}_{\text{tune}}$ are empirical estimates on D_{tune} . Only $\hat{\phi}_{\text{tune}}$ is carried forward. The tuning threshold $\hat{\lambda}_{\text{tune}}$ is used only to rank candidate structures on D_{tune} and is discarded before deployment. The deployed threshold is the split-conformal quantile computed on the independent calibration split D_{cal} . Since $\hat{\phi}_{\text{tune}}$ does not depend on D_{cal} , the standard exchangeability argument of split CP applies directly.

Theorem 3.1 (Finite-sample marginal coverage of DCO-Warmstart). *Assume that*

$$(X_1, Y_1), \dots, (X_m, Y_m), (X_{m+1}, Y_{m+1})$$

are exchangeable conditional on D_{train} and D_{tune} , and that $\hat{\phi}_{\text{tune}}$ is measurable with respect to $D_{\text{train}} \cup D_{\text{tune}}$ only. Let

$$S_i = S_{\hat{\phi}_{\text{tune}}}(X_i, Y_i), \quad i = 1, \dots, m,$$

let $S_{(1)} \leq \dots \leq S_{(m)}$ denote the sorted calibration scores, and define

$$k_{\alpha} = \lceil (m+1)(1-\alpha) \rceil, \quad \hat{q}_{1-\alpha} = \begin{cases} S_{(k_{\alpha})}, & k_{\alpha} \leq m, \\ +\infty, & k_{\alpha} = m+1. \end{cases}$$

Then

$$\mathbb{P}\{Y_{m+1} \in C_{\hat{\phi}_{\text{tune}, \hat{q}_{1-\alpha}}}(X_{m+1})\} \geq 1 - \alpha.$$

This guarantee holds for any candidate class Φ , finite or infinite, because calibration is applied only after a single tuned structure has been fixed independently of D_{cal} .

3.3 Sample Complexity

We do not claim an end-to-end finite-sample oracle guarantee for the final recalibrated DCO-Warmstart predictor. Instead, we give a finite-class uniform-convergence result for the tuning stage alone, which explains when the tuning split is large enough to select an efficient candidate structure before the independent conformal calibration step is applied.

Proposition 3.2 (Tuning oracle inequality for a finite search class). *Let \mathcal{A} be a finite class of candidate prediction-set rules, where each $a \in \mathcal{A}$ defines a set-valued predictor C_a . Let*

$$R(a) = \mathbb{P}\{Y \notin C_a(X)\}, \quad S(a) = \mathbb{E}[s(C_a(X))]$$

denote its miscoverage risk and expected size, where $s(C_a(X)) \in [0, B]$. Let $\widehat{R}_{\text{tune}}(a)$ and $\widehat{S}_{\text{tune}}(a)$ be the corresponding empirical quantities on m_{tune} independent tuning samples. Fix $\varepsilon_R, \varepsilon_S, \eta > 0$. With probability at least $1 - \eta$, uniformly over $a \in \mathcal{A}$,

$$\left| \widehat{R}_{\text{tune}}(a) - R(a) \right| \leq \varepsilon_R, \quad \left| \widehat{S}_{\text{tune}}(a) - S(a) \right| \leq \varepsilon_S,$$

provided

$$m_{\text{tune}} \geq \max \left\{ \frac{\log(4|\mathcal{A}|/\eta)}{2\varepsilon_R^2}, \frac{B^2 \log(4|\mathcal{A}|/\eta)}{2\varepsilon_S^2} \right\}.$$

Consequently, if the tuning rule selects

$$\widehat{a} \in \arg \min_{a \in \mathcal{A}} \widehat{S}_{\text{tune}}(a) \quad \text{s.t.} \quad \widehat{R}_{\text{tune}}(a) \leq \alpha - \varepsilon_R,$$

then, on the same event

$$R(\widehat{a}) \leq \alpha$$

and

$$S(\widehat{a}) \leq \inf_{a \in \mathcal{A}: R(a) \leq \alpha - 2\varepsilon_R} S(a) + 2\varepsilon_S.$$

Interpretation. The final deployed DCO-Warmstart set is still calibrated on D_{cal} , so its finite-sample marginal coverage does not rely on the empirical feasibility event in the proposition. The proposition instead explains when the tuning split is large enough to select an efficient structure before the independent conformal calibration step is applied. Calibration accuracy can be analysed separately once the tuned structure is fixed. Appendix B gives a Dvoretzky–Kiefer–Wolfowitz-based lemma showing that, under local regularity around the population quantile, the empirical conformal quantile concentrates around its population target at rate $m_{\text{cal}}^{-1/2}$.

3.4 Asymptotic Agreement with CRC/BQ

Proposition 3.3 (Asymptotic agreement under uniform risk-bound consistency). *Fix a structure ϕ and write*

$$R(\lambda) = \mathbb{P}\{Y \notin C_{\phi, \lambda}(X)\}.$$

Assume:

1. $R(\lambda)$ is continuous and strictly decreasing in a neighbourhood of

$$\lambda^* = \inf\{\lambda : R(\lambda) \leq \alpha\}.$$

2. The split-conformal DCO-Warmstart threshold satisfies

$$\hat{\lambda}_{\text{DCO}} \xrightarrow{p} \lambda^*.$$

3. The coupled CRC/BQ threshold can be written as

$$\hat{\lambda}_{\text{CRC}} = \inf\{\lambda : \hat{R}_m(\lambda) + b_m(\lambda, \delta_m) \leq \alpha\},$$

where

$$\sup_{\lambda \in \Lambda} |\hat{R}_m(\lambda) - R(\lambda)| \xrightarrow{p} 0, \quad \sup_{\lambda \in \Lambda} b_m(\lambda, \delta_m) \xrightarrow{p} 0.$$

Then

$$\hat{\lambda}_{\text{CRC}} - \hat{\lambda}_{\text{DCO}} \xrightarrow{p} 0.$$

Assumption 2 is the standard consistency requirement for the split-conformal quantile. It holds under mild local regularity of the score distribution; in particular, Lemma B.3 in Appendix B gives a DKW-based concentration bound for $\hat{q}_{1-\alpha}$ around its population quantile. Thus the proposition should be read as a comparison of large-sample targets, not as an equivalence of finite-sample guarantees.

Interpretation. DCO-Warmstart gives finite-sample marginal conformal coverage, whereas CRC/BQ-style methods give high-probability risk control. Proposition 3.3 only states that, when the coupled risk bound consistently estimates the population risk boundary and its excess margin vanishes, the selected thresholds approach the same population limit.

4 Decoupled Conformal Optimisation

Building on Section 3, we describe the operational procedure for DCO-Warmstart. As shown in Figure 1, the key departure from BCP is the introduction of a dedicated tuning split D_{tune} : structural selection and conformal calibration are allocated to independent data splits, so the exchangeability argument of Theorem 3.1 applies without modification.

4.1 Data Splitting and Tuning

Given exchangeable data D_n , we partition it into three disjoint splits D_{train} , D_{tune} , and D_{cal} , as defined in Section 3. The posterior $\pi(\theta | D_{\text{train}})$ is estimated on D_{train} , thereby fixing the score function $S_\phi(x, y)$ with respect to all subsequent splits. In the BCP setting, $S_\phi(x, y) = -\log p(y | x, D_{\text{train}})$ is the negative log posterior predictive density, and ϕ encodes structural choices such as the score type, prior hyperparameters, or model architecture.

On D_{tune} , we compute the empirical miscoverage and average set size,

$$\hat{R}_{\text{tune}}(\phi, \lambda) = \frac{1}{|D_{\text{tune}}|} \sum_{(X_i, Y_i) \in D_{\text{tune}}} \mathbf{1}\{Y_i \notin C_{\phi, \lambda}(X_i)\}, \quad (7)$$

$$\hat{S}_{\text{tune}}(\phi, \lambda) = \frac{1}{|D_{\text{tune}}|} \sum_{(X_i, Y_i) \in D_{\text{tune}}} |C_{\phi, \lambda}(X_i)|, \quad (8)$$

where λ denotes a candidate threshold used to form the tentative prediction set $C_{\phi, \lambda}(x)$ during tuning. We then select structural choices by solving

$$(\hat{\phi}_{\text{tune}}, \hat{\lambda}_{\text{tune}}) = \arg \min_{(\phi, \lambda) \in \Phi \times \Lambda} \hat{S}_{\text{tune}}(\phi, \lambda) \quad \text{s.t.} \quad \hat{R}_{\text{tune}}(\phi, \lambda) \leq \alpha. \quad (9)$$

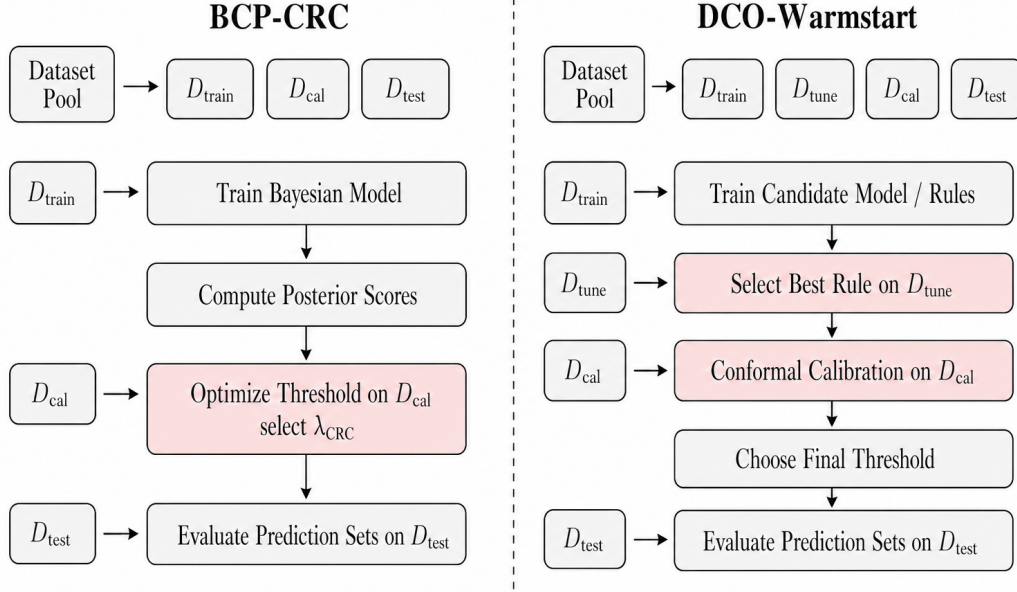


Figure 1: Coupled calibration versus DCO-Warmstart. In CRC/BQ-style calibration, the same calibration split is used both to search for an efficient threshold and to certify risk. DCO-Warmstart separates these roles: D_{tune} is used for score/model/hyperparameter selection, while D_{cal} is reserved exclusively for the final conformal quantile. This separation is the key condition that allows the standard split-conformal exchangeability argument to apply after tuning.

In practice, (9) is solved by grid search over $\Phi \times \Lambda$; the monotonicity of $\widehat{R}_{\text{tune}}(\phi, \cdot)$ in λ permits an efficient line search for each fixed ϕ . If no candidate pair satisfies the constraint $\widehat{R}_{\text{tune}}(\phi, \lambda) \leq \alpha$, we select the candidate with the smallest empirical miscoverage, breaking ties in favor of smaller average set size.

It is important to note the distinct roles of the two outputs of (9). The selected structure $\hat{\phi}_{\text{tune}}$ is carried forward as the chosen model configuration. The accompanying threshold $\hat{\lambda}_{\text{tune}}$, however, serves purely as a ranking device during the search over Φ : it identifies how tight a threshold is needed for each candidate ϕ to satisfy the empirical miscoverage constraint on D_{tune} , thereby ranking candidates by their empirical efficiency. The threshold $\hat{\lambda}_{\text{tune}}$ is *not* deployed. Instead, the deployed threshold is the conformal quantile

$$\hat{q}_{1-\alpha} = \text{Quantile} \left(\{S_{\hat{\phi}_{\text{tune}}}(X_i, Y_i)\}_{(X_i, Y_i) \in D_{\text{cal}}}, \frac{\lceil (1-\alpha)(|D_{\text{cal}}| + 1) \rceil}{|D_{\text{cal}}|} \right), \quad (10)$$

computed afresh on the held-out calibration set D_{cal} . Because $\hat{\phi}_{\text{tune}}$ is determined using only D_{train} and D_{tune} , and is not adapted to D_{cal} , the marginal coverage guarantee of Theorem 3.1 applies to the prediction set $C_{\hat{\phi}_{\text{tune}}, \hat{q}_{1-\alpha}}$. We refer to this two-stage procedure—tuning over (ϕ, λ) pairs on D_{tune} to select the structure, then recalibrating on D_{cal} to obtain the deployed threshold—as **DCO-Warmstart**.

4.2 DCO-Warmstart: Structure Selection with Conformal Calibration

Once the structure $\hat{\phi}_{\text{tune}}$ has been selected on D_{tune} , the deployed threshold is determined entirely by the held-out calibration set D_{cal} . Let $D_{\text{cal}} = \{(X_i, Y_i)\}_{i=1}^m$, define the calibration scores

$$S_i = S_{\hat{\phi}_{\text{tune}}}(X_i, Y_i), \quad i = 1, \dots, m,$$

and let

$$S_{(1)} \leq \dots \leq S_{(m)}$$

denote the sorted calibration scores. Define

$$k_\alpha = \lceil (m+1)(1-\alpha) \rceil.$$

The exact split-conformal calibration threshold is then

$$\hat{q}_{1-\alpha} = \begin{cases} S_{(k_\alpha)}, & k_\alpha \leq m, \\ +\infty, & k_\alpha = m+1. \end{cases} \quad (11)$$

The resulting prediction set is

$$C_{\text{DCO}}(x) = \{y : S_{\hat{\phi}_{\text{tune}}}(x, y) \leq \hat{q}_{1-\alpha}\}. \quad (12)$$

By Theorem 3.1, this prediction set satisfies finite-sample marginal coverage. This is the primary certified procedure used throughout the paper. At deployment, the method uses only the structure selected on D_{tune} together with the conformal calibration threshold computed on D_{cal} ; all tuning thresholds, including $\hat{\lambda}_{\text{tune}}$, are discarded.

Algorithm 1 DCO-Warmstart: Structure Selection with Conformal Calibration

Require: Data D_n , miscoverage level α , candidate structure class Φ , threshold grid Λ

- 1: Partition D_n into D_{train} , D_{tune} , and D_{cal}
- 2: Estimate posterior $\pi(\theta \mid D_{\text{train}})$ and define scores $\{S_\phi\}_{\phi \in \Phi}$
- 3: Solve (9) on D_{tune} to obtain $(\hat{\phi}_{\text{tune}}, \hat{\lambda}_{\text{tune}})$
- 4: Discard $\hat{\lambda}_{\text{tune}}$ and retain only $\hat{\phi}_{\text{tune}}$
- 5: Compute $S_i = S_{\hat{\phi}_{\text{tune}}}(X_i, Y_i)$ for each $(X_i, Y_i) \in D_{\text{cal}}$
- 6: Sort S_1, \dots, S_m into $S_{(1)} \leq \dots \leq S_{(m)}$
- 7: Set $k_\alpha = \lceil (m+1)(1-\alpha) \rceil$
- 8: Set

$$\hat{q}_{1-\alpha} = \begin{cases} S_{(k_\alpha)}, & k_\alpha \leq m, \\ +\infty, & k_\alpha = m+1 \end{cases}$$

Ensure: $C_{\text{DCO}}(x) = \{y : S_{\hat{\phi}_{\text{tune}}}(x, y) \leq \hat{q}_{1-\alpha}\}$

4.3 DirectTune

As a diagnostic baseline, we also consider a direct threshold-tuning procedure. Unlike DCO-Warmstart, DirectTune does not perform structure selection followed by recalibration. Instead, for a fixed externally chosen structure $\phi_0 \in \Phi$ and its corresponding score function S_{ϕ_0} , it optimizes the threshold on D_{tune} and deploys that threshold directly. Specifically, DirectTune selects

$$\hat{\lambda}_{\text{tune}} \in \arg \min_{\lambda \in \Lambda} \hat{S}_{\text{tune}}(\phi_0, \lambda) \quad \text{s.t.} \quad \hat{R}_{\text{tune}}(\phi_0, \lambda) \leq \alpha, \quad (13)$$

and deploys the prediction set

$$C_{\text{DirectTune}}(x) = \{y : S_{\phi_0}(x, y) \leq \hat{\lambda}_{\text{tune}}\}. \quad (14)$$

DirectTune is not conformally certified. Because the threshold is selected using the same data on which feasibility is evaluated, the empirical constraint on D_{tune} does not imply finite-sample marginal coverage for future test points. We therefore use DirectTune only as a diagnostic baseline to quantify the cost of omitting the final calibration step.

Algorithm 2 DirectTune

Require: Data D_n , miscoverage level α , fixed structure ϕ_0 , score function S_{ϕ_0} , threshold grid Λ

- 1: Partition D_n into D_{train} and D_{tune} {No calibration split; hence no conformal guarantee}
- 2: Estimate posterior $\pi(\theta | D_{\text{train}})$ and fix the score function S_{ϕ_0}
- 3: Solve (13) on D_{tune} to obtain $\hat{\lambda}_{\text{tune}}$

Ensure: $C_{\text{DirectTune}}(x) = \{y : S_{\phi_0}(x, y) \leq \hat{\lambda}_{\text{tune}}\}$

4.4 Computational Complexity

In practice, DCO-Warmstart scales linearly with the number of candidate structures $K = |\Phi|$. For a calibration split of size m_{cal} , the final conformal calibration step requires $\mathcal{O}(m_{\text{cal}} \log m_{\text{cal}})$ operations due to sorting the calibration scores. The tuning cost depends on the threshold search strategy. Assuming that the per-point score evaluation cost is $\mathcal{O}(1)$, a direct grid search over $\Phi \times \Lambda$ requires $\mathcal{O}(K|\Lambda|m_{\text{tune}})$ operations. The monotonicity of $\hat{R}_{\text{tune}}(\phi, \cdot)$ in λ can reduce this cost by permitting an efficient line search for each fixed ϕ . In the BCP setting, the cost of evaluating the posterior predictive density $p(y | x, D_{\text{train}})$ may dominate this bookkeeping cost, depending on the posterior approximation and the number of posterior samples used.

For a finite candidate class, the tuning-stage oracle inequality in Proposition 3.2 requires

$$m_{\text{tune}} = \Omega\left(\max\left\{\frac{\log(K/\eta)}{\varepsilon_R^2}, \frac{B^2 \log(K/\eta)}{\varepsilon_S^2}\right\}\right), \quad (15)$$

for uniform control of empirical miscoverage and empirical size across candidates, where ε_R and ε_S denote the desired uniform deviations for miscoverage and size, B bounds the prediction-set size functional, and η is the failure probability. This tuning-stage result controls the quality of structure selection. The final finite-sample marginal coverage guarantee is supplied separately by Theorem 3.1 through the independent calibration split D_{cal} .

5 Experiments

We evaluate DCO-Warmstart on regression and classification tasks. We use *certified* to denote methods equipped with a formal risk or coverage guarantee under their respective calibration procedures (e.g., conformal marginal coverage for DCO-Warmstart and high-probability risk control guarantees for BQ). Throughout, we use δ to denote the failure probability and $1 - \delta$ the confidence level for risk-control methods; BQ is run with $\delta = 0.05$, corresponding to confidence 0.95. Where prior BQ literature uses β for the confidence level, we set $\beta = 1 - \delta$ to align notation.

Full model specification and implementation details are in Appendix C. DCO-Warmstart serves as the primary certified method, DirectTune as a diagnostic baseline, and BQ (Snell and Griffiths,

2025) as the closest methodological comparator; Split CP and CQR serve as standard predictive baselines. DCO-Warmstart and BQ are evaluated over 50 random splits using each method’s own calibration protocol; statistical reliability is assessed via paired Wilcoxon signed-rank tests.

Matched comparison protocol. To isolate the effect of decoupling from the effect of candidate search, we report several matched-budget controls. Since BQ/CRC-style calibration does not natively perform the same structural search as DCO-Warmstart, we separate three comparisons. First, we compare fixed-structure DCO-Warmstart and fixed-structure BQ/CRC using the same score/model configuration. Second, we select a structure using DCO-Warmstart on D_{tune} and then recalibrate that fixed structure using the BQ/CRC risk-control protocol on its combined calibration pool; this isolates the calibration mechanism after holding the selected structure fixed. Third, we report an exploratory matched- Φ BQ/CRC extension, in which BQ/CRC is evaluated over the same candidate class used by DCO-Warmstart. These controls distinguish candidate search, calibration mechanism, and data-budget allocation.

Experimental reporting. For each dataset and target coverage level, we report empirical coverage¹, average prediction-set size or interval width, and the 95th percentile of set size or interval width. All results are averaged over repeated random splits. When comparing DCO-Warmstart and BQ/CRC on the same splits, we report paired Wilcoxon signed-rank tests for size and coverage differences. Since DCO-Warmstart and BQ/CRC target different guarantees, we interpret these tests descriptively rather than as evidence that one guarantee dominates the other.

5.1 Regression: Diabetes Dataset

Setup. We use the Diabetes dataset ($n = 442$, $d = 10$) with target coverage $1 - \alpha = 0.8$. Each run partitions the data into four disjoint splits with approximate sizes $|D_{\text{train}}| \approx 150$, $|D_{\text{tune}}| \approx 112$, $|D_{\text{cal}}| \approx 113$, $|D_{\text{test}}| \approx 67$. A sparse Bayesian linear regression model is fitted on D_{train} via NUTS MCMC with $T = 8,000$ posterior samples; Split CP and CQR are included as standard predictive baselines alongside BQ. Full specifications are in Appendix C.2.

DCO-Warmstart pipeline. DCO-Warmstart proceeds in two stages on D_{tune} , independent of D_{cal} . First, the prior scale $c \in \{1.0, 0.02\}$ is selected by evaluating empirical coverage and interval width; $c = 1.0$ is chosen as the most efficient feasible option in 28 of 50 splits. Second, the scalar threshold λ is optimised by minimising average interval width subject to empirical coverage $\geq 1 - \alpha$. The selected $\hat{\lambda}_{\text{tune}}$ is then conformally recalibrated on D_{cal} , yielding certified DCO-Warmstart intervals; DirectTune applies $\hat{\lambda}_{\text{tune}}$ directly without recalibration.

Results. Table 2 summarises coverage and interval width over 50 splits. Across methods, BQ is systematically more conservative than Split CP in both coverage and interval width (Figure 5), reflecting the additional margin introduced by its high-probability calibration criterion. DCO-Warmstart achieves empirical coverage close to the target (0.805 ± 0.066) and produces among the narrowest certified intervals (1.914 ± 0.192), with both differences relative to BQ statistically significant (paired Wilcoxon; see caption). Direct tuning matches DCO-Warmstart’s average width but without a coverage guarantee, exhibiting higher per-split variance consistent with Remark B.2.

¹Empirical coverage on a finite test split can fall slightly below the nominal level even when the procedure satisfies a finite-sample marginal coverage guarantee. The guarantee concerns the probability over future exchangeable test points and data splits, not deterministic coverage on every realised finite test set.

Figure 2 further shows that DCO-Warmstart concentrates tightly around the nominal level, sitting between the underconservative direct tuning and the overconservative BQ.

Table 2: Regression results on the Diabetes dataset over 50 random splits (target $1 - \alpha = 0.8$). Paired Wilcoxon p -values (DCO-Warmstart vs. BQ, $n = 50$): width $p = 3.09 \times 10^{-12}$, coverage $p = 2.36 \times 10^{-7}$.

Method	Coverage	Avg. Interval Width	Certified
BQ	0.842 ± 0.051	2.098 ± 0.131	✓
Split CP	0.812 ± 0.057	1.920 ± 0.159	✓
CQR	0.807 ± 0.060	1.990 ± 0.159	✓
DCO-Warmstart	0.805 ± 0.066	1.914 ± 0.192	✓
DirectTune	0.805 ± 0.072	1.914 ± 0.163	×

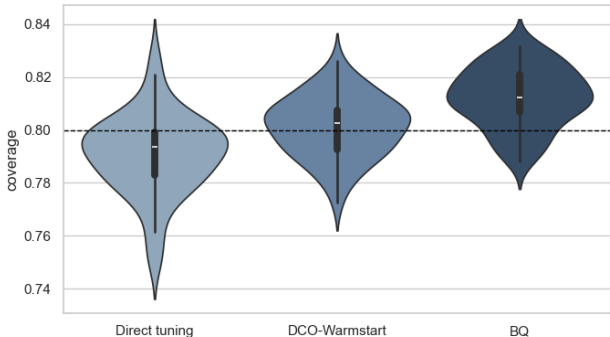


Figure 2: Coverage (a) and interval width (b) on the Diabetes dataset over 50 random splits ($1 - \alpha = 0.8$). The dashed line marks the target level.

5.2 Classification: ImageNet-A

Setup. We evaluate DCO-Warmstart on a filtered subset of ImageNet-A (198 classes) with target coverage $1 - \alpha = 0.8$, using a pretrained ResNet-50 backbone with a two-layer MC-dropout classification head ($T = 20$ stochastic forward passes). Data are partitioned into approximately 2000 samples each for training, calibration, and testing, and 1000 for tuning, across 50 stratified random seeds. DCO-Warmstart searches over score type (`posterior_nll` or `aoi_nll`), dropout rate $\in \{0.05, 0.1, 0.2, 0.3\}$, and hidden width $\in \{(512, 256), (256, 128)\}$, giving $|\Phi| = 16$ candidates. Full specifications are in Appendix C.3.1.

Results. DCO-Warmstart tracks the nominal coverage level closely (0.801 vs target 0.8), reduces the average prediction set from 26.52 to 25.26, and narrows the P95 tail from 58.95 to 53.73, with all three differences statistically significant (Table 3). DirectTune achieves smaller sets but falls below the nominal coverage level in this classification experiment (0.791 vs. target 0.8), consistent with Remark B.2. Per-seed selection frequencies are in Table 12.

Single-run illustration. Table 4 traces the threshold progression for a representative seed. The tuning threshold $\lambda_{\text{tune}} = 6.18$ falls below the nominal coverage target when applied directly for this seed; recalibration raises it to $q_{\text{cal}} = 6.42$, restoring coverage to 0.797. BQ selects the more

Table 3: ImageNet-A classification over 50 random splits (target $1 - \alpha = 0.8$). Paired Wilcoxon p -values (DCO-Warmstart vs. BQ, $n = 50$): coverage $p = 9.34 \times 10^{-9}$, average set size $p = 9.77 \times 10^{-9}$, P95 set size $p = 1.69 \times 10^{-9}$.

Method	Coverage	Avg. Set Size	P95 Set Size
BQ	0.812 ± 0.011	26.52 ± 1.34	58.95 ± 3.04
DCO-Warmstart	0.801 ± 0.011	25.26 ± 1.60	53.73 ± 3.11
DirectTune	0.791 ± 0.015	23.83 ± 1.80	50.65 ± 4.02

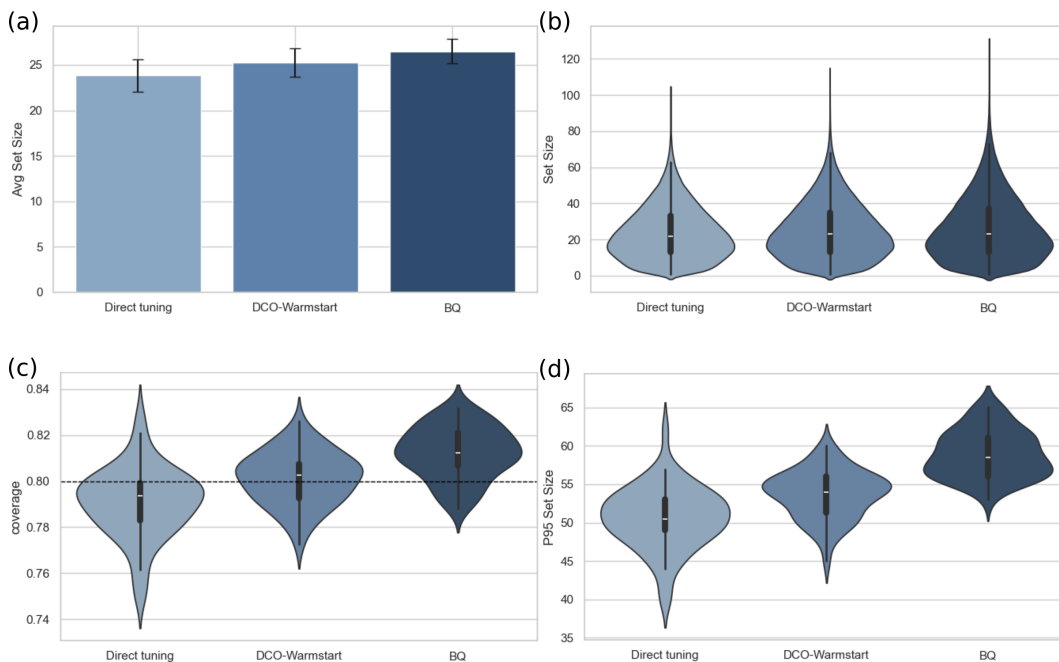


Figure 3: Classification results on ImageNet-A over 50 random splits. (a) Mean prediction set size. (b) Set size distributions. (c) Empirical coverage; dashed line marks $1 - \alpha = 0.8$. (d) P95 set size distributions.

conservative $\lambda_{BQ} = 6.510$, recovering higher coverage (0.808) at the cost of 4% larger prediction sets. The achieved BQ feasibility probability at this threshold is $\hat{p}_{BQ} = \hat{\mathbb{P}}(L^+ \leq \alpha) = 0.954 > 1 - \delta = 0.95$, confirming that BQ satisfies its risk-control constraint with a small margin above the nominal confidence level.

Discussion. The two experiments tell a consistent story. Where the candidate space is large and the tuning signal strong, as in classification, DCO-Warmstart’s efficiency gains over BQ are pronounced; where it is smaller and noisier, as in regression, the advantage is more modest but persists. In both cases, the core insight holds: decoupling optimisation from calibration is not only theoretically valid but empirically beneficial, freeing the tuning stage to select more efficient prediction rules while retaining the finite-sample marginal coverage guarantee of split conformal calibration.

Additional ablations. To further isolate the effect of decoupling, we additionally report ablations over candidate search, split allocation, and target coverage level. These ablations support a practical

Table 4: Single-seed threshold progression on ImageNet-A. Conformal recalibration raises the tuning threshold from λ_{tune} to q_{cal} , restoring the split-conformal coverage guarantee. BQ selects a more conservative threshold λ_{BQ} . Here $\hat{p}_{\text{BQ}} = \hat{\mathbb{P}}(L^+ \leq \alpha)$ is the achieved posterior feasibility probability estimated by Dirichlet sampling. It can exceed the nominal confidence level 0.95 because BQ selects the smallest feasible threshold rather than enforcing equality.

	λ_{tune}	q_{cal}	λ_{BQ}	\hat{p}_{BQ}
Threshold	6.180	6.419	6.510	0.954
Method	Coverage	Avg. Size	P95	
DCO-Warmstart	0.797	24.56	54.0	
BQ	0.808	25.56	56.0	

split-allocation principle: for a fixed non-training budget, the tuning split should be large enough to stabilise candidate selection, while the remaining data should be allocated to calibration to reduce conformal-quantile variability.

Table 5: Matched candidate-class and calibration-mechanism controls on ImageNet-A. Because BQ/CRC does not natively include DCO-style structural search, we report fixed-structure baselines, BQ/CRC recalibration after DCO-Warmstart-selected structure, and an exploratory matched- Φ BQ/CRC extension. These comparisons should be read as diagnostic controls rather than as a claim that BQ/CRC and DCO-Warmstart implement identical search procedures.

Method	Candidate class	Coverage	Avg. size/width	P95 size/width
BQ/CRC, fixed ϕ	fixed	0.8122 ± 0.0112	26.5192 ± 1.3438	58.9460 ± 3.0425
DCO-Warmstart, fixed ϕ	fixed	0.8025 ± 0.0108	25.0450 ± 1.3687	55.6630 ± 3.1192
Exploratory matched- Φ BQ/CRC	matched Φ	0.8196 ± 0.0116	28.0215 ± 1.8460	59.8660 ± 3.6270
DCO-Warmstart, search over Φ	matched Φ	0.8013 ± 0.0114	25.2584 ± 1.5990	53.7260 ± 3.1137
DirectTune	matched Φ	0.7908 ± 0.0151	23.8286 ± 1.8024	50.6460 ± 4.0233

Table 6: DCO-Warmstart split-ratio ablation. The total non-training budget $|D_{\text{tune}}| + |D_{\text{cal}}|$ is fixed, while the allocation between tuning and calibration varies. The current codebase provides the 20/80, 33/67, 50/50, 67/33, and 80/20 settings; selected-candidate stability is reported as the fraction of seeds choosing the modal candidate.

Tune/calibration ratio	Coverage	Avg. size/width	P95 size/width	Selected candidate stability
20/80	0.8001 ± 0.0121	25.1344 ± 1.6044	52.7240 ± 2.7653	32.0%
33/67	0.8013 ± 0.0114	25.2584 ± 1.5990	53.7260 ± 3.1137	48.0%
50/50	0.7996 ± 0.0122	24.9321 ± 1.5405	52.9460 ± 3.7823	46.0%
67/33	0.8010 ± 0.0141	25.0379 ± 1.8596	53.6030 ± 4.2108	52.0%
80/20	0.8027 ± 0.0168	25.2462 ± 2.6829	53.8880 ± 5.7259	48.0%

Table 5 shows that the exploratory matched- Φ BQ/CRC control produces a larger average set size than the fixed-structure BQ/CRC baseline (28.02 versus 26.52). The increase mainly comes from data allocation: part of the non-training budget is used for tuning, leaving less effective calibration information for the high-probability risk constraint and leading to a more conservative threshold. DCO-Warmstart avoids this by separating candidate ranking on D_{tune} from final calibration on D_{cal} , keeping its average set size stable at 25.26.

Split-allocation principle. DCO-Warmstart introduces an allocation trade-off absent from standard split CP. Given a fixed non-training budget $m = m_{\text{tune}} + m_{\text{cal}}$, the tuning split controls the stability of structural selection, while the calibration split controls the variability of the final conformal quantile. If the best candidate is well separated, a small tuning split may suffice; if several candidates have similar efficiency, more tuning data may be needed.

Table 6 evaluates this trade-off on ImageNet-A. Coverage and average set size remain stable across all five allocations, with coverage ranging from 0.7996 to 0.8027 and average set size from 24.93 to 25.26. Candidate stability rises from 32% under the 20/80 split to 48% under the 33/67 split, then fluctuates between 46% and 52% for larger tuning fractions. In contrast, the standard deviation of the P95 set size increases as D_{cal} shrinks, from 2.77 at 20/80 to 5.73 at 80/20. These results suggest a simple rule: increase m_{tune} until candidate selection stabilises, then allocate the remaining data to D_{cal} . On ImageNet-A, the 33/67 split provides a good balance, achieving near-maximal candidate stability while keeping the P95 variability close to its minimum.

Table 7: Performance across target coverage levels. Reporting multiple α values tests whether DCO-Warmstart remains reliable beyond the single $1 - \alpha = 0.8$ setting.

Dataset	Target coverage	Method	Empirical coverage	Avg. size/width
ImageNet-A	0.80	BQ/CRC	0.8122 ± 0.0112	26.5192 ± 1.3438
ImageNet-A	0.80	DCO-Warmstart	0.8012 ± 0.0109	25.2442 ± 1.5561
ImageNet-A	0.90	BQ/CRC	0.9093 ± 0.0075	49.3689 ± 2.1015
ImageNet-A	0.90	DCO-Warmstart	0.9014 ± 0.0080	46.8652 ± 2.1532
ImageNet-A	0.95	BQ/CRC	0.9580 ± 0.0053	74.4952 ± 3.1281
ImageNet-A	0.95	DCO-Warmstart	0.9515 ± 0.0067	71.2709 ± 3.6914
CIFAR-100	0.80	BQ/CRC	0.8110 ± 0.0106	2.7219 ± 0.1434
CIFAR-100	0.80	DCO-Warmstart	0.7994 ± 0.0125	2.5270 ± 0.1634
CIFAR-100	0.90	BQ/CRC	0.9071 ± 0.0087	5.8332 ± 0.4278
CIFAR-100	0.90	DCO-Warmstart	0.8978 ± 0.0101	5.3802 ± 0.4791
CIFAR-100	0.95	BQ/CRC	0.9547 ± 0.0060	10.7320 ± 0.7601
CIFAR-100	0.95	DCO-Warmstart	0.9488 ± 0.0085	10.0229 ± 1.2058

Table 8: Additional regression benchmarks across target coverage levels on California Housing and Concrete. Both BQ/CRC and DCO-Warmstart are reported using completed reruns under the matched-budget protocol.

Dataset	Target coverage	Method	Empirical coverage	Avg. width
California Housing	0.80	BQ/CRC	0.8080 ± 0.0273	1.3507 ± 0.0472
California Housing	0.80	DCO-Warmstart	0.7902 ± 0.0287	1.2917 ± 0.0558
California Housing	0.90	BQ/CRC	0.9112 ± 0.0185	1.9377 ± 0.0867
California Housing	0.90	DCO-Warmstart	0.8996 ± 0.0205	1.8339 ± 0.0932
California Housing	0.95	BQ/CRC	0.9586 ± 0.0118	2.7078 ± 0.1572
California Housing	0.95	DCO-Warmstart	0.9511 ± 0.0144	2.5302 ± 0.1768
Concrete	0.80	BQ/CRC	0.8226 ± 0.0432	1.7109 ± 0.0818
Concrete	0.80	DCO-Warmstart	0.7934 ± 0.0490	1.5821 ± 0.1278
Concrete	0.90	BQ/CRC	0.9195 ± 0.0309	2.2582 ± 0.1000
Concrete	0.90	DCO-Warmstart	0.8937 ± 0.0316	2.0915 ± 0.1252
Concrete	0.95	BQ/CRC	0.9640 ± 0.0188	2.7371 ± 0.1268
Concrete	0.95	DCO-Warmstart	0.9462 ± 0.0252	2.5274 ± 0.1579

6 Conclusion

We studied whether optimisation and final conformal calibration must use the same held-out data in Bayesian conformal optimisation pipelines. When the target is finite-sample marginal conformal coverage, they need not. Decoupled Conformal Optimisation (DCO) assigns these roles to separate splits. The tuning split selects the score, model, prior, or threshold-search configuration. The calibration split is then used only to compute the final conformal quantile.

This separation preserves the standard split-conformal logic. Once the tuned structure is fixed independently of D_{cal} , the calibration scores and the test score remain exchangeable. Theorem 3.1 therefore gives finite-sample marginal coverage for any candidate class Φ , without a confidence parameter and without a multiple-testing correction over the candidate class. Proposition 3.2 complements this result by describing when the tuning split is large enough to select an efficient candidate from a finite class. Proposition 3.3 provides a large-sample comparison: under consistency assumptions on the coupled risk bound, DCO-Warmstart and CRC/BQ-style calibration converge to the same population threshold, although their finite-sample guarantees remain distinct.

This distinction is important. DCO-Warmstart is not a replacement for CRC/BQ-style methods when the scientific goal is high-probability risk control. Those methods provide a different type of guarantee, controlled by a confidence level $1 - \delta$. DCO-Warmstart is aimed at the marginal coverage setting. In that setting, coupling optimisation and calibration is sufficient but not necessary. An independent tuning split can be used for efficiency-oriented search, while a fresh calibration split supplies the conformal coverage guarantee.

The experiments support this view. Under matched protocols, DCO-Warmstart retains the split-conformal marginal coverage guarantee and, in finite test evaluations, tracks the nominal level closely while often producing smaller prediction sets or intervals than coupled high-probability calibration baselines. On ImageNet-A, the average set size decreases from 26.52 to 25.26, with the 95th-percentile set size decreasing from 58.95 to 53.73, indicating improvement in the tail of the set-size distribution. On the Diabetes regression benchmark, the average interval width decreases from 2.098 to 1.914. DirectTune illustrates the cost of omitting the final calibration step: it may

achieve smaller sets at the cost of under-coverage or increased coverage variability, since it lacks a finite-sample conformal guarantee.

6.1 Limitations and future work.

DCO-Warmstart introduces a practical allocation problem. Data must be divided among training, tuning, and calibration, and the best split ratio depends on the task. The tuning split should be large enough to stabilise candidate selection. The calibration split should remain large enough to reduce quantile variability. A simple diagnostic is to monitor whether the selected $\hat{\phi}_{\text{tune}}$ changes under repeated random splits of the tuning data. Stability of this selection suggests that the tuning budget is sufficient; the remaining non-training data can then be allocated to calibration.

Several theoretical questions remain open. The current tuning-stage oracle result covers finite candidate classes. Extensions to adaptive split allocation, continuous hyperparameter spaces, and end-to-end efficiency after recalibration would make the theory more complete. The asymptotic comparison in Proposition 3.3 also relies on consistency of the coupled risk bound. Understanding when this condition holds for specific CRC/BQ constructions, and how large the finite-sample conservativeness gap remains for fixed δ , are useful directions for future work.

Acknowledgement

This work was supported by the Engineering and Physical Sciences Research Council (EPSRC) under Grant No. EP/Y030826/1.

References

- A. N. Angelopoulos and S. Bates. A gentle introduction to conformal prediction and distribution-free uncertainty quantification, 2022. URL <https://arxiv.org/abs/2107.07511>.
- A. N. Angelopoulos, S. Bates, J. Malik, and M. I. Jordan. Uncertainty sets for image classifiers using conformal prediction. In *International Conference on Learning Representations (ICLR)*, 2021. URL https://openreview.net/forum?id=eNdiU_DbM9.
- A. N. Angelopoulos, S. Bates, E. J. Candès, M. I. Jordan, and L. Lei. Learn then test: Calibrating predictive algorithms to achieve risk control. *The Annals of Applied Statistics*, 19(2):1641 – 1662, 2025a. doi: 10.1214/24-AOAS1998. URL <https://doi.org/10.1214/24-AOAS1998>.
- A. N. Angelopoulos, S. Bates, A. Fisch, L. Lei, and T. Schuster. Conformal risk control, 2025b. URL <https://arxiv.org/abs/2208.02814>.
- R. F. Barber, E. J. Candès, A. Ramdas, and R. J. Tibshirani. Conformal prediction beyond exchangeability. *The Annals of Statistics*, 51(2):816 – 845, 2023. doi: 10.1214/23-AOS2276. URL <https://doi.org/10.1214/23-AOS2276>.
- A. Bellotti. Optimized conformal classification using gradient descent approximation. *CoRR*, abs/2105.11255, 2021. URL <https://arxiv.org/abs/2105.11255>.
- M. Caprio. The joys of categorical conformal prediction, 2025. URL <https://arxiv.org/abs/2507.04441>.
- M. Caprio, S. Dutta, K. J. Jang, V. Lin, R. Ivanov, O. Sokolsky, and I. Lee. Credal bayesian deep learning. *Transactions on Machine Learning Research*, 2024. ISSN 2835-8856. URL <https://openreview.net/forum?id=4NHF9AC5ui>.
- M. Caprio, D. Stutz, S. Li, and A. Doucet. Conformalized credal regions for classification with ambiguous ground truth. *Transactions on Machine Learning Research*, 2025. ISSN 2835-8856. URL <https://openreview.net/forum?id=L7sQ8CW2FY>.
- G. S. Dhillon, G. Deligiannidis, and T. Rainforth. On the expected size of conformal prediction sets, 2024. URL <https://arxiv.org/abs/2306.07254>.
- E. Fong and C. C. Holmes. Conformal bayesian computation. In *Advances in Neural Information Processing Systems (NeurIPS)*, volume 34, pages 18268–18279, 2021. URL <https://openreview.net/forum?id=e95xWq07ehi>.
- J. Lei, M. G’Sell, A. Rinaldo, R. J. Tibshirani, and L. Wasserman. Distribution-free predictive inference for regression. *Journal of the American Statistical Association*, 113(523):1094–1111, 2018.
- M. Sadinle, J. Lei, and L. Wasserman. Least ambiguous set-valued classifiers with bounded error levels. *Journal of the American Statistical Association*, 114(525):223–234, 2018. ISSN 1537-274X. doi: 10.1080/01621459.2017.1395341. URL <http://dx.doi.org/10.1080/01621459.2017.1395341>.
- G. Shafer and V. Vovk. A tutorial on conformal prediction. *Journal of Machine Learning Research*, 9:371–421, 2008. URL <https://arxiv.org/abs/0706.3188>.

- J. C. Snell and T. L. Griffiths. Conformal prediction as bayesian quadrature, 2025. URL <https://openreview.net/forum?id=PNmkjIzHB7>.
- V. Vovk, A. Gammerman, and G. Shafer. *Algorithmic Learning in a Random World*. Springer, 2005.
- T. Wang and E. Dobriban. Optimal decision-making based on prediction sets, 2026. URL <https://arxiv.org/abs/2602.00989>.
- F. Wu, V. Lohmanova, S. Kaski, and M. Caprio. Bayesian conformal prediction as a decision risk problem, 2026. URL <https://arxiv.org/abs/2602.03331>.

A Split Conformal Prediction

Algorithm 3 summarises the standard split conformal prediction pipeline. The procedure requires no assumptions beyond exchangeability of the data and a bounded non-conformity score, and the coverage guarantee follows directly from the order statistics of the calibration scores.

Algorithm 3 Split Conformal Prediction

Require: Training data D_{train} , calibration data D_{cal} , miscoverage level α

- 1: Train model \hat{f} on D_{train}
- 2: Compute non-conformity scores $S_i = S(X_i, Y_i)$ for each $(X_i, Y_i) \in D_{\text{cal}}$
- 3: Sort S_1, \dots, S_m into $S_{(1)} \leq \dots \leq S_{(m)}$
- 4: Set $k_\alpha = \lceil (m+1)(1-\alpha) \rceil$
- 5: Set $\hat{q}_{1-\alpha} = S_{(k_\alpha)}$ if $k_\alpha \leq m$, and $\hat{q}_{1-\alpha} = +\infty$ otherwise

Ensure: $C(x) = \{y : S(x, y) \leq \hat{q}_{1-\alpha}\}$, which satisfies $\mathbb{P}(Y_{n+1} \in C(X_{n+1})) \geq 1 - \alpha$

The marginal coverage guarantee follows from a standard exchangeability argument. Since the calibration points and the test point (X_{n+1}, Y_{n+1}) are exchangeable, the test non-conformity score S_{n+1} is equally likely to fall at any rank among S_1, \dots, S_m, S_{n+1} . Therefore,

$$\mathbb{P}(Y_{n+1} \in C(X_{n+1})) = \mathbb{P}(S_{n+1} \leq \hat{q}_{1-\alpha}) \geq 1 - \alpha. \quad (16)$$

Crucially, $\hat{q}_{1-\alpha}$ is an order statistic of D_{cal} and involves no optimisation; the efficiency of $C(x)$ therefore depends entirely on the expressiveness of the non-conformity score $S(x, y)$.

B Proofs and Technical Details

This appendix provides complete proofs for all theoretical results stated in Section 3, together with supporting lemmas and extensions.

B.1 Proof of Theorem 3.1 (Marginal Coverage of DCO-Warmstart)

Proof. Let $\hat{\phi}_{\text{tune}}$ be selected using D_{train} and D_{tune} only. Let $D_{\text{cal}} = \{(X_i, Y_i)\}_{i=1}^m$, and define the calibration scores

$$S_i = S_{\hat{\phi}_{\text{tune}}}(X_i, Y_i), \quad i = 1, \dots, m. \quad (17)$$

Define the test score as

$$S_{m+1} = S_{\hat{\phi}_{\text{tune}}}(X_{m+1}, Y_{m+1}). \quad (18)$$

Let

$$S_{(1)} \leq \dots \leq S_{(m)} \quad (19)$$

denote the sorted calibration scores, and define

$$k_\alpha = \lceil (m+1)(1-\alpha) \rceil. \quad (20)$$

The split-conformal calibration threshold is

$$\hat{q}_{1-\alpha} = \begin{cases} S_{(k_\alpha)}, & k_\alpha \leq m, \\ +\infty, & k_\alpha = m+1. \end{cases} \quad (21)$$

Since $\hat{\phi}_{\text{tune}}$ depends only on D_{train} and D_{tune} , and is not adapted to D_{cal} , the score function $S_{\hat{\phi}_{\text{tune}}}(\cdot, \cdot)$ is fixed with respect to the calibration data. Conditional on D_{train} , D_{tune} , and $\hat{\phi}_{\text{tune}}$, the calibration points and the test point,

$$(X_1, Y_1), \dots, (X_m, Y_m), (X_{m+1}, Y_{m+1}), \quad (22)$$

are exchangeable. Therefore, the scores

$$S_1, \dots, S_m, S_{m+1} \quad (23)$$

are exchangeable conditional on D_{train} , D_{tune} , and $\hat{\phi}_{\text{tune}}$.

By the standard split-conformal coverage argument Vovk et al. (2005); Shafer and Vovk (2008), exchangeability of the scores implies

$$\mathbb{P}(S_{m+1} \leq \hat{q}_{1-\alpha} \mid D_{\text{train}}, D_{\text{tune}}, \hat{\phi}_{\text{tune}}) \geq 1 - \alpha. \quad (24)$$

Since

$$Y_{m+1} \in C_{\hat{\phi}_{\text{tune}}, \hat{q}_{1-\alpha}}(X_{m+1}) \iff S_{m+1} \leq \hat{q}_{1-\alpha}, \quad (25)$$

taking expectations over D_{train} , D_{tune} , and $\hat{\phi}_{\text{tune}}$ gives

$$\mathbb{P}(Y_{m+1} \in C_{\hat{\phi}_{\text{tune}}, \hat{q}_{1-\alpha}}(X_{m+1})) \geq 1 - \alpha. \quad (26)$$

□

Remark B.1 (Score selection and multiple testing). The argument above holds for any candidate class Φ , finite or infinite. The key requirement is that calibration is applied to a single fixed structure $\hat{\phi}_{\text{tune}}$ selected without using D_{cal} . Unlike procedures that select among multiple thresholds using the calibration data, DCO-Warmstart does not require a union bound or family-wise error correction over Φ for its final conformal coverage guarantee.

Remark B.2 (Failure of DirectTune). DirectTune selects

$$\hat{\lambda}_{\text{tune}} = \arg \min_{\lambda} \hat{\mathcal{S}}_{\text{tune}}(\lambda) \quad \text{s.t.} \quad \hat{R}_{\text{tune}}(\lambda) \leq \alpha, \quad (27)$$

and deploys this threshold directly without further calibration. This procedure is not conformally certified. For any fixed λ , the empirical risk $\hat{R}_{\text{tune}}(\lambda)$ estimates the corresponding population risk $R(\lambda)$. However, the selected threshold $\hat{\lambda}_{\text{tune}}$ is itself a function of D_{tune} . Thus, the same data are used both to choose the threshold and to certify its empirical feasibility. This selection effect can introduce optimistic bias, so the empirical feasibility constraint does not imply finite-sample marginal coverage for future test points. In finite samples, this can manifest as undercoverage or increased coverage variability.

B.2 Proof of Proposition 3.2 (Tuning oracle inequality for a finite search class)

Proof. Let \mathcal{A} denote a finite search class, where each $a \in \mathcal{A}$ represents a candidate procedure, such as a pair $a = (\phi, \lambda)$. Define its population miscoverage and population size by

$$R(a) = \mathbb{P}\{Y \notin C_a(X)\}, \quad \mathcal{S}(a) = \mathbb{E}[s(C_a(X))], \quad (28)$$

and their empirical counterparts on D_{tune} by

$$\hat{R}_{\text{tune}}(a) = \frac{1}{m_{\text{tune}}} \sum_{i=1}^{m_{\text{tune}}} \mathbf{1}\{Y_i \notin C_a(X_i)\}, \quad (29)$$

and

$$\widehat{\mathcal{S}}_{\text{tune}}(a) = \frac{1}{m_{\text{tune}}} \sum_{i=1}^{m_{\text{tune}}} s(C_a(X_i)). \quad (30)$$

Assume that the size functional is bounded as

$$0 \leq s(C_a(X)) \leq B \quad \text{for all } a \in \mathcal{A}. \quad (31)$$

For each fixed $a \in \mathcal{A}$, the random variable $\mathbf{1}\{Y \notin C_a(X)\}$ is bounded in $[0, 1]$. Hoeffding's inequality gives

$$\mathbb{P}\left(\left|\widehat{R}_{\text{tune}}(a) - R(a)\right| > \varepsilon_R\right) \leq 2 \exp(-2m_{\text{tune}}\varepsilon_R^2). \quad (32)$$

Applying a union bound over $a \in \mathcal{A}$ yields

$$\mathbb{P}\left(\sup_{a \in \mathcal{A}} \left|\widehat{R}_{\text{tune}}(a) - R(a)\right| > \varepsilon_R\right) \leq 2|\mathcal{A}| \exp(-2m_{\text{tune}}\varepsilon_R^2). \quad (33)$$

Similarly, since $s(C_a(X))/B \in [0, 1]$, Hoeffding's inequality gives

$$\mathbb{P}\left(\left|\widehat{\mathcal{S}}_{\text{tune}}(a) - \mathcal{S}(a)\right| > \varepsilon_S\right) \leq 2 \exp\left(-\frac{2m_{\text{tune}}\varepsilon_S^2}{B^2}\right). \quad (34)$$

A second union bound over $a \in \mathcal{A}$ yields

$$\mathbb{P}\left(\sup_{a \in \mathcal{A}} \left|\widehat{\mathcal{S}}_{\text{tune}}(a) - \mathcal{S}(a)\right| > \varepsilon_S\right) \leq 2|\mathcal{A}| \exp\left(-\frac{2m_{\text{tune}}\varepsilon_S^2}{B^2}\right). \quad (35)$$

Therefore, if

$$m_{\text{tune}} \geq \max\left\{\frac{\log(4|\mathcal{A}|/\eta)}{2\varepsilon_R^2}, \frac{B^2 \log(4|\mathcal{A}|/\eta)}{2\varepsilon_S^2}\right\}, \quad (36)$$

then with probability at least $1 - \eta$, the following two uniform deviation bounds hold simultaneously:

$$\sup_{a \in \mathcal{A}} \left|\widehat{R}_{\text{tune}}(a) - R(a)\right| \leq \varepsilon_R, \quad (37)$$

and

$$\sup_{a \in \mathcal{A}} \left|\widehat{\mathcal{S}}_{\text{tune}}(a) - \mathcal{S}(a)\right| \leq \varepsilon_S. \quad (38)$$

On this event, let \widehat{a} be an empirical minimizer of average size subject to the empirical miscoverage constraint:

$$\widehat{a} \in \arg \min_{a \in \mathcal{A}} \widehat{\mathcal{S}}_{\text{tune}}(a) \quad \text{s.t.} \quad \widehat{R}_{\text{tune}}(a) \leq \alpha. \quad (39)$$

Then its population miscoverage satisfies

$$R(\widehat{a}) \leq \widehat{R}_{\text{tune}}(\widehat{a}) + \varepsilon_R \leq \alpha + \varepsilon_R. \quad (40)$$

Moreover, any candidate $a \in \mathcal{A}$ satisfying

$$R(a) \leq \alpha - \varepsilon_R \quad (41)$$

is empirically feasible, because

$$\widehat{R}_{\text{tune}}(a) \leq R(a) + \varepsilon_R \leq \alpha. \quad (42)$$

Hence, for every such candidate a , the empirical minimizer satisfies

$$\widehat{\mathcal{S}}_{\text{tune}}(\widehat{a}) \leq \widehat{\mathcal{S}}_{\text{tune}}(a). \quad (43)$$

Using the uniform size deviation bound on both sides gives

$$\mathcal{S}(\widehat{a}) \leq \widehat{\mathcal{S}}_{\text{tune}}(\widehat{a}) + \varepsilon_S \leq \widehat{\mathcal{S}}_{\text{tune}}(a) + \varepsilon_S \leq \mathcal{S}(a) + 2\varepsilon_S. \quad (44)$$

Taking the infimum over all candidates satisfying $R(a) \leq \alpha - \varepsilon_R$ yields

$$\mathcal{S}(\widehat{a}) \leq \inf_{a \in \mathcal{A}: R(a) \leq \alpha - \varepsilon_R} \mathcal{S}(a) + 2\varepsilon_S. \quad (45)$$

Thus, with probability at least $1 - \eta$, the selected candidate has population miscoverage at most $\alpha + \varepsilon_R$ and size within $2\varepsilon_S$ of the best candidate whose population miscoverage is at most $\alpha - \varepsilon_R$.

If one instead uses the tightened empirical constraint

$$\widehat{R}_{\text{tune}}(a) \leq \alpha - \varepsilon_R, \quad (46)$$

then the same argument gives the stronger feasibility statement

$$R(\widehat{a}) \leq \alpha, \quad (47)$$

with the oracle comparison taken over candidates satisfying

$$R(a) \leq \alpha - 2\varepsilon_R. \quad (48)$$

This proves the proposition. \square

Possible extension. An extension to infinite or continuous candidate classes would require additional uniform-convergence machinery, such as covering-number or empirical-process arguments, together with explicit regularity assumptions on the search class. We leave such extensions to future work and do not claim them in the present paper.

B.3 Calibration Quantile Accuracy

Lemma B.3 (Calibration quantile accuracy). *Fix a tuned structure $\widehat{\phi}_{\text{tune}}$ and let $F_{\widehat{\phi}_{\text{tune}}}$ denote the distribution function of $S_{\widehat{\phi}_{\text{tune}}}(X, Y)$. Define the population quantile*

$$q_{\widehat{\phi}_{\text{tune}}}^* = \inf \left\{ q : F_{\widehat{\phi}_{\text{tune}}}(q) \geq 1 - \alpha \right\}. \quad (49)$$

Let $m = m_{\text{cal}}$, let $S_{(1)} \leq \dots \leq S_{(m)}$ denote the sorted calibration scores, and define

$$k_\alpha = \lceil (m + 1)(1 - \alpha) \rceil. \quad (50)$$

Assume that $k_\alpha \leq m$, and let

$$\widehat{q}_{1-\alpha} = S_{(k_\alpha)}. \quad (51)$$

Suppose that $F_{\widehat{\phi}_{\text{tune}}}$ is continuous and has density bounded below by $c > 0$ in a neighbourhood of $q_{\widehat{\phi}_{\text{tune}}}^*$. Then, for any $t > 0$ such that $q_{\widehat{\phi}_{\text{tune}}}^* \pm t$ remain in this neighbourhood,

$$\mathbb{P} \left(\left| \widehat{q}_{1-\alpha} - q_{\widehat{\phi}_{\text{tune}}}^* \right| > t \right) \leq 2 \exp \left\{ -2m \left(ct - \frac{2}{m} \right)_+^2 \right\}, \quad (52)$$

where $(u)_+ = \max\{u, 0\}$. In particular, if $ct > 2/m$, the right-hand side decays exponentially in mt^2 .

Proof. Let

$$p = 1 - \alpha. \quad (53)$$

Let \widehat{F}_m be the empirical distribution function of the m calibration scores. By the Dvoretzky–Kiefer–Wolfowitz inequality,

$$\mathbb{P}\left(\sup_q \left| \widehat{F}_m(q) - F_{\hat{\phi}_{\text{tune}}}(q) \right| > \epsilon\right) \leq 2 \exp(-2m\epsilon^2). \quad (54)$$

Because

$$k_\alpha = \lceil (m+1)p \rceil, \quad (55)$$

we have

$$\frac{k_\alpha}{m} \leq p + \frac{2}{m}. \quad (56)$$

Moreover, since $k_\alpha \geq (m+1)p$, we also have

$$\frac{k_\alpha}{m} \geq p. \quad (57)$$

By the lower density assumption, for $q_{\hat{\phi}_{\text{tune}}}^* + t$ in the stated neighbourhood,

$$F_{\hat{\phi}_{\text{tune}}}(q_{\hat{\phi}_{\text{tune}}}^* + t) \geq p + ct. \quad (58)$$

If $\hat{q}_{1-\alpha} > q_{\hat{\phi}_{\text{tune}}}^* + t$, then fewer than k_α calibration scores are less than or equal to $q_{\hat{\phi}_{\text{tune}}}^* + t$, and hence

$$\widehat{F}_m(q_{\hat{\phi}_{\text{tune}}}^* + t) < \frac{k_\alpha}{m}. \quad (59)$$

Combining this with (56) and (58) gives

$$\sup_q \left| \widehat{F}_m(q) - F_{\hat{\phi}_{\text{tune}}}(q) \right| > ct - \frac{2}{m}. \quad (60)$$

Similarly, by the lower density assumption, for $q_{\hat{\phi}_{\text{tune}}}^* - t$ in the stated neighbourhood,

$$F_{\hat{\phi}_{\text{tune}}}(q_{\hat{\phi}_{\text{tune}}}^* - t) \leq p - ct. \quad (61)$$

If $\hat{q}_{1-\alpha} < q_{\hat{\phi}_{\text{tune}}}^* - t$, then at least k_α calibration scores are less than or equal to $q_{\hat{\phi}_{\text{tune}}}^* - t$, and hence

$$\widehat{F}_m(q_{\hat{\phi}_{\text{tune}}}^* - t) \geq \frac{k_\alpha}{m}. \quad (62)$$

Using (57) and (61), this implies

$$\sup_q \left| \widehat{F}_m(q) - F_{\hat{\phi}_{\text{tune}}}(q) \right| > ct. \quad (63)$$

Combining (60) and (63), we obtain

$$\left\{ \left| \hat{q}_{1-\alpha} - q_{\hat{\phi}_{\text{tune}}}^* \right| > t \right\} \subseteq \left\{ \sup_q \left| \widehat{F}_m(q) - F_{\hat{\phi}_{\text{tune}}}(q) \right| > \left(ct - \frac{2}{m} \right)_+ \right\}. \quad (64)$$

Applying (54) with

$$\epsilon = \left(ct - \frac{2}{m} \right)_+ \quad (65)$$

gives (52). \square

B.4 Proof of Proposition 3.3 (Asymptotic Agreement under Uniform Risk-Bound Consistency)

We restate the regularity conditions for completeness.

Assumption B.4. (A1) The function $R(\lambda)$ is continuous and strictly decreasing in a neighbourhood of

$$\lambda^* = \inf \{ \lambda : R(\lambda) \leq \alpha \}. \quad (66)$$

Moreover, λ^* is an interior point of the search domain Λ .

(A2) The split-conformal DCO-Warmstart threshold satisfies

$$\hat{\lambda}_{\text{DCO}} \xrightarrow{p} \lambda^*. \quad (67)$$

(A3) The coupled CRC/BQ threshold can be written as

$$\hat{\lambda}_{\text{CRC}} = \inf \left\{ \lambda : \hat{R}_m(\lambda) + b_m(\lambda, \delta_m) \leq \alpha \right\}, \quad (68)$$

where $b_m(\lambda, \delta_m) \geq 0$ and the empirical risk and excess margin satisfy, respectively,

$$\sup_{\lambda \in \Lambda} \left| \hat{R}_m(\lambda) - R(\lambda) \right| \xrightarrow{p} 0, \quad (69)$$

and

$$\sup_{\lambda \in \Lambda} b_m(\lambda, \delta_m) \xrightarrow{p} 0. \quad (70)$$

Proof of Proposition 3.3. By assumption (A2),

$$\hat{\lambda}_{\text{DCO}} \xrightarrow{p} \lambda^*. \quad (71)$$

It remains to show that

$$\hat{\lambda}_{\text{CRC}} \xrightarrow{p} \lambda^*. \quad (72)$$

Fix any $\varepsilon > 0$ small enough that $\lambda^* - \varepsilon$ and $\lambda^* + \varepsilon$ lie in the neighbourhood where R is continuous and strictly decreasing. Since λ^* is the boundary of the population feasible set and R is strictly decreasing near λ^* , we have

$$R(\lambda^* - \varepsilon) > \alpha > R(\lambda^* + \varepsilon). \quad (73)$$

Define the positive margin

$$\Delta_\varepsilon = \frac{1}{2} \min \{ R(\lambda^* - \varepsilon) - \alpha, \alpha - R(\lambda^* + \varepsilon) \} > 0. \quad (74)$$

By assumption (A3), with probability tending to one,

$$\sup_{\lambda \in \Lambda} \left| \hat{R}_m(\lambda) - R(\lambda) \right| \leq \Delta_\varepsilon \quad (75)$$

and

$$\sup_{\lambda \in \Lambda} b_m(\lambda, \delta_m) \leq \Delta_\varepsilon. \quad (76)$$

On this event, since $b_m(\lambda, \delta_m) \geq 0$,

$$\hat{R}_m(\lambda^* - \varepsilon) + b_m(\lambda^* - \varepsilon, \delta_m) \geq R(\lambda^* - \varepsilon) - \Delta_\varepsilon > \alpha. \quad (77)$$

Thus $\lambda^* - \varepsilon$ is not feasible. Similarly,

$$\widehat{R}_m(\lambda^* + \varepsilon) + b_m(\lambda^* + \varepsilon, \delta_m) \leq R(\lambda^* + \varepsilon) + 2\Delta_\varepsilon < \alpha. \quad (78)$$

Thus $\lambda^* + \varepsilon$ is feasible. Therefore, on an event whose probability tends to one,

$$\lambda^* - \varepsilon < \widehat{\lambda}_{\text{CRC}} \leq \lambda^* + \varepsilon. \quad (79)$$

Equivalently,

$$\left| \widehat{\lambda}_{\text{CRC}} - \lambda^* \right| \leq \varepsilon \quad (80)$$

with probability tending to one. Hence,

$$\widehat{\lambda}_{\text{CRC}} \xrightarrow{p} \lambda^*. \quad (81)$$

Combining this with assumption (A2) yields

$$\widehat{\lambda}_{\text{DCO}} - \widehat{\lambda}_{\text{CRC}} \xrightarrow{p} 0. \quad (82)$$

□

Remark B.5 (Finite-sample distinction between DCO-Warmstart and CRC/BQ). Proposition 3.3 should not be interpreted as asserting that DCO-Warmstart and CRC/BQ provide the same finite-sample guarantee. They do not. DCO-Warmstart targets marginal conformal coverage, whereas CRC/BQ targets high-probability risk control. The proposition states only that, when the coupled risk bound consistently estimates the population risk boundary and its excess margin $b_m(\lambda, \delta_m)$ vanishes uniformly, the selected thresholds approach a common population limit λ^* .

Remark B.6 (Verifying Assumption 2 via Lemma B.3). Assumption 2 is not an additional hypothesis imposed on the method; it is a consequence of the standard split-conformal quantile construction under mild regularity. Specifically, Lemma B.3 shows that, if the score distribution $F_{\widehat{\phi}_{\text{tune}}}$ is continuous and has density bounded below by $c > 0$ in a neighbourhood of the population quantile $q_{\widehat{\phi}_{\text{tune}}}^*$, then the empirical conformal threshold $\widehat{q}_{1-\alpha}$ satisfies

$$\mathbb{P}\left(|\widehat{q}_{1-\alpha} - q_{\widehat{\phi}_{\text{tune}}}^*| > t\right) \leq 2 \exp\left(-2m_{\text{cal}}\left(ct - \frac{2}{m_{\text{cal}}}\right)_+^2\right),$$

which implies $\widehat{q}_{1-\alpha} \xrightarrow{p} q_{\widehat{\phi}_{\text{tune}}}^*$ as $m_{\text{cal}} \rightarrow \infty$. Identifying $\widehat{\lambda}_{\text{DCO}} = \widehat{q}_{1-\alpha}$ and $\lambda^* = q_{\widehat{\phi}_{\text{tune}}}^*$, Assumption 2 therefore holds whenever the score distribution satisfies the local density condition of Lemma B.3. The correction term $(ct - 2/m_{\text{cal}})_+$ accounts for the discreteness of the order statistic and is negligible once $m_{\text{cal}} \gg 1/(ct)$.

C Experimental Details and Additional Results

This appendix provides full implementation details and additional results for the experiments in Section 5. Appendix C.2 covers the regression experiment and Appendix C.3 covers the ImageNet-A classification experiment.

C.1 Shared Experimental Components

Matched-budget protocol. For all datasets, BQ/CRC uses the union $D_{\text{tune}} \cup D_{\text{cal}}$ as its calibration pool, so both DCO-Warmstart and the coupled baseline consume the same total number of non-training examples. DCO-Warmstart allocates these examples across two independent splits; BQ/CRC treats them as a single pool and applies its own risk-control procedure.

BQ/CRC implementation. The BQ threshold is selected as

$$\hat{\lambda}_{\text{BQ}} = \inf\{\lambda : \mathbb{P}(L^+(\lambda) \leq \alpha \mid \ell_{1:m}(\lambda)) \geq 1 - \delta\}, \quad (83)$$

where L^+ is the Dirichlet-MC upper bound on conformal risk. Unless stated otherwise, all BQ/CRC runs use $\delta = 0.05$ (confidence $1 - \delta = 0.95$), $M = 1,000$ Dirichlet draws, and maximum loss bound $B = 1.0$.

C.2 Regression Experiments

Shared model specification. All regression experiments use the same sparse Bayesian linear regression family:

$$Y \mid X, \theta, \theta_0, \tau \sim \mathcal{N}(X^\top \theta + \theta_0, \tau), \quad (84)$$

with hierarchical priors

$$\theta_j \sim \text{Laplace}(0, b), \quad b \sim \text{Gamma}(1, 1), \quad \tau \sim \text{HalfNormal}(c), \quad \theta_0 \sim \mathcal{N}(0, 10). \quad (85)$$

The non-conformity score is the posterior predictive negative log-likelihood,

$$S(x, y) = -\log \hat{p}(y \mid x), \quad \log \hat{p}(y \mid x) = \log \left(\frac{1}{T} \sum_{t=1}^T p(y \mid x, \theta^{(t)}) \right), \quad (86)$$

where $\theta^{(t)}$ are NUTS MCMC posterior draws. Prediction intervals are formed on a response grid spanning $[\min(y_{\text{train}}) - 2, \max(y_{\text{train}}) + 2]$. Inputs X and targets y are standardised with `StandardScaler`. DCO-Warmstart searches over prior scale $c \in \{1.0, 0.02\}$; BQ/CRC uses a fixed structure with $c = 1.0$.

Non-Bayesian baselines (Diabetes only). *Split CP.* A ridge regressor \hat{f} is trained on D_{train} . Calibration residuals are $s_i = |y_i - \hat{f}(x_i)|$ for $(x_i, y_i) \in D_{\text{cal}}$, and the prediction interval is $C(x) = [\hat{f}(x) - q, \hat{f}(x) + q]$ where $q = \text{Quantile}_{1-\alpha}\{s_i\}$.

CQR. Lower and upper quantile regressors $\hat{q}_{\alpha/2}, \hat{q}_{1-\alpha/2}$ (gradient boosting, 200 estimators, max depth 3) are trained on D_{train} . Calibration scores are

$$s_i = \max(\hat{q}_{\alpha/2}(x_i) - y_i, y_i - \hat{q}_{1-\alpha/2}(x_i)), \quad (87)$$

and the interval is $[\hat{q}_{\alpha/2}(x) - q, \hat{q}_{1-\alpha/2}(x) + q]$ where $q = \text{Quantile}_{1-\alpha}\{s_i\}$.

C.2.1 Diabetes

Data splitting. Each run partitions $n = 442$ observations into approximate sizes $|D_{\text{train}}| \approx 150$, $|D_{\text{tune}}| \approx 112$, $|D_{\text{cal}}| \approx 113$, $|D_{\text{test}}| \approx 67$, repeated over 50 random seeds.

MCMC settings. $T = 8,000$ posterior samples after warm-up; response grid size $B = 400$.

Hyperparameter selection. Table 9 reports calibrated test performance for both prior scales. Both values yield nearly identical coverage and width after conformal recalibration, indicating that the calibration step absorbs the effect of prior misspecification on this dataset.

Table 9: Prior scale selection on the Diabetes dataset (mean \pm std over 50 splits, target $1 - \alpha = 0.8$). Conformal recalibration on D_{cal} absorbs the effect of prior misspecification.

Prior scale c	Coverage	Width
$c = 1.0$	0.841 ± 0.063	2.051 ± 0.238
$c = 0.02$	0.843 ± 0.061	2.047 ± 0.231

Table 10: DCO-Warmstart threshold-selection outcomes on D_{tune} across 50 splits.

Outcome	Count (out of 50)
Feasible λ found	50
Fallback (no feasible λ)	0

Threshold-selection outcomes. Table 10 summarises the λ -optimisation outcomes across 50 splits. A feasible λ satisfying empirical coverage $\geq 1 - \alpha$ was found in every split; the fallback was never triggered.

DirectTune diagnostic. The tuning-based threshold produces intervals of identical average width to the calibration quantile (1.914 vs. 1.914) but with higher per-split coverage variance (0.072 vs. 0.066 std), consistent with the optimistic bias of Remark B.2.

C.2.2 California Housing

Data source and splitting. Loaded via `sklearn.datasets.fetch_california_housing`; rows with non-finite values are removed and the pool is subsampled to 3,000 observations. After removing 15% as D_{test} (≈ 450), the remaining budget is split 30%/30%/rest into D_{tune} , D_{cal} (≈ 765 each), and D_{train} ($\approx 1,020$). BQ/CRC calibrates on the combined pool of $\approx 1,530$ points.

MCMC settings. 600 warm-up steps, 3,000 posterior samples, 1 chain; response grid of 300 points. Both DCO-Warmstart and BQ/CRC use identical MCMC settings.

C.2.3 Concrete Compressive Strength

Data source. Loaded from OpenML (`Concrete_Compressive_Strength`, version 3); if unavailable, the UCI Excel file is used as a fallback. Rows with missing or non-numeric values are dropped; no subsampling is applied.

Data splitting. Same proportional protocol as California Housing: 15% test, 30% tuning, 30% calibration, remainder for training.

MCMC settings. Both DCO-Warmstart and BQ/CRC use identical posterior inference settings: 600 warm-up steps, 3,000 posterior samples, 1 chain, and a response grid of 300 points. This matched configuration is used for all three target coverage levels reported in Table 8.

C.3 Classification Experiments

Shared backbone and scoring. Both ImageNet-A and CIFAR-100 experiments use a pretrained ResNet-50 as a frozen feature extractor, with an MC-dropout classification head trained on D_{train} . Predictive uncertainty is approximated via $T = 20$ stochastic forward passes (model kept in `train` mode). Two nonconformity scores are evaluated for each candidate:

$$\bar{p}(c | x) = \frac{1}{T} \sum_{t=1}^T p_t(c | x), \quad S_{\text{post}}(x, c) = -\log \bar{p}(c | x), \quad (88)$$

$$\tilde{p}(c | x) = \frac{\sum_t p_t(c | x)^2}{\sum_t p_t(c | x)}, \quad S_{\text{aoi}}(x, c) = -\log \tilde{p}(c | x). \quad (89)$$

Both scores induce nested prediction sets $C_\lambda(x) = \{y : S(x, y) \leq \lambda\}$.

Shared DCO-Warmstart candidate class. DCO-Warmstart searches over $|\Phi| = 16$ configurations:

- score type: `posterior_nll`, `aoi_nll`;
- dropout rate: $\{0.05, 0.10, 0.20, 0.30\}$;
- hidden widths: $\{(512, 256), (256, 128)\}$.

For each candidate the tuning-stage threshold is searched over 80 quantile-based values derived from D_{tune} ; ties are broken by P95 set size then by λ value. The deployed threshold is recalibrated on D_{cal} using the exact split-conformal quantile.

Shared BQ/CRC baseline. The baseline uses a fixed structure (`posterior_nll`, dropout 0.05, hidden (512, 256)) and calibrates on the combined pool $D_{\text{tune}} \cup D_{\text{cal}}$, with $\delta = 0.05$, $B = 1.0$, and $M = 1,000$ Dirichlet draws.

C.3.1 ImageNet-A

Data splitting. Data are partitioned into approximately 2,000 samples each for D_{train} , D_{cal} , and D_{test} , and 1,000 for D_{tune} , across 50 stratified random seeds (198 classes). The BQ/CRC calibration pool therefore contains 3,000 points.

Candidate configurations and selection. Table 11 lists all 16 configurations evaluated on D_{tune} for a representative seed. All configurations achieve the target coverage (0.8) on the tuning split; DCO-Warmstart selects `cand_001` (posterior NLL, dropout 0.05, hidden (512, 256)) as it achieves the smallest average set size (22.105) among feasible candidates. Table 12 summarises selection frequencies across all 50 seeds.

Single-run illustration. For the representative seed in Table 11, the tuning threshold $\lambda_{\text{tune}} = 6.180$ falls below the nominal target when applied directly; recalibration on D_{cal} raises it to $q_{\text{cal}} = 6.419$, restoring coverage to 0.797. BQ selects the more conservative threshold $\lambda_{\text{BQ}} = 6.510$, achieving coverage 0.808 at the cost of larger sets (25.56 vs. 24.56).

C.3.2 CIFAR-100

Data source. Raw images are loaded from `torchvision.datasets.CIFAR100` (training and test partitions concatenated into a single pool); a pretrained ResNet-50 (`ResNet50_Weights.DEFAULT`) is used as a frozen feature extractor with the final classification layer removed.

Table 11: Top 10 candidate configurations evaluated on D_{tune} for ImageNet-A (representative seed). All configurations are feasible; selected configuration in bold.

ID	Score	Dropout	Hidden	λ	Status	Avg Size	P95
cand_001	posterior_nll	0.05	(512,256)	6.180	feasible	22.105	49.00
cand_003	posterior_nll	0.10	(512,256)	6.095	feasible	22.216	49.00
cand_009	aoi_nll	0.05	(512,256)	5.725	feasible	22.238	47.00
cand_011	aoi_nll	0.10	(512,256)	5.337	feasible	22.363	46.00
cand_005	posterior_nll	0.20	(512,256)	6.016	feasible	23.587	49.00
cand_007	posterior_nll	0.30	(512,256)	5.872	feasible	24.519	48.00
cand_010	aoi_nll	0.05	(256,128)	5.568	feasible	24.880	49.05
cand_008	posterior_nll	0.30	(256,128)	5.443	feasible	25.138	46.00
cand_004	posterior_nll	0.10	(256,128)	6.083	feasible	25.141	51.00
cand_002	posterior_nll	0.05	(256,128)	6.336	feasible	25.583	55.00

Table 12: DCO-Warmstart candidate selection frequencies on D_{tune} across 50 seeds on ImageNet-A. All 16 configurations achieved the coverage constraint in every seed (infeasible fallback: 0/50).

Score type	Hidden dims	Dropout	Seeds selected	%
aoi_nll	(512, 256)	0.05	20	40%
posterior_nll	(512, 256)	0.05	12	24%
posterior_nll	(512, 256)	0.10	7	14%
aoi_nll	(512, 256)	0.10	4	8%
posterior_nll	(512, 256)	0.20	4	8%
posterior_nll	(256, 128)	0.05	1	2%
posterior_nll	(256, 128)	0.30	1	2%
aoi_nll	(256, 128)	0.05	1	2%
<i>Marginal: score type</i>				
aoi_nll			25	50%
posterior_nll			25	50%
<i>Marginal: hidden dims</i>				
(512, 256)			47	94%
(256, 128)			3	6%
<i>Marginal: dropout rate</i>				
0.05			34	68%
0.10			11	22%
0.20			4	8%
0.30			1	2%

Classification head training. Adam optimiser, learning rate 10^{-3} , weight decay 10^{-4} , batch size 128, 15 epochs.

Data splitting. For each of 50 random seeds: $|D_{\text{train}}| = 2,000$, $|D_{\text{tune}}| = 1,000$, $|D_{\text{cal}}| = 2,000$, $|D_{\text{test}}| = 2,000$. The BQ/CRC calibration pool therefore contains 3,000 points, matching the ImageNet-A protocol.

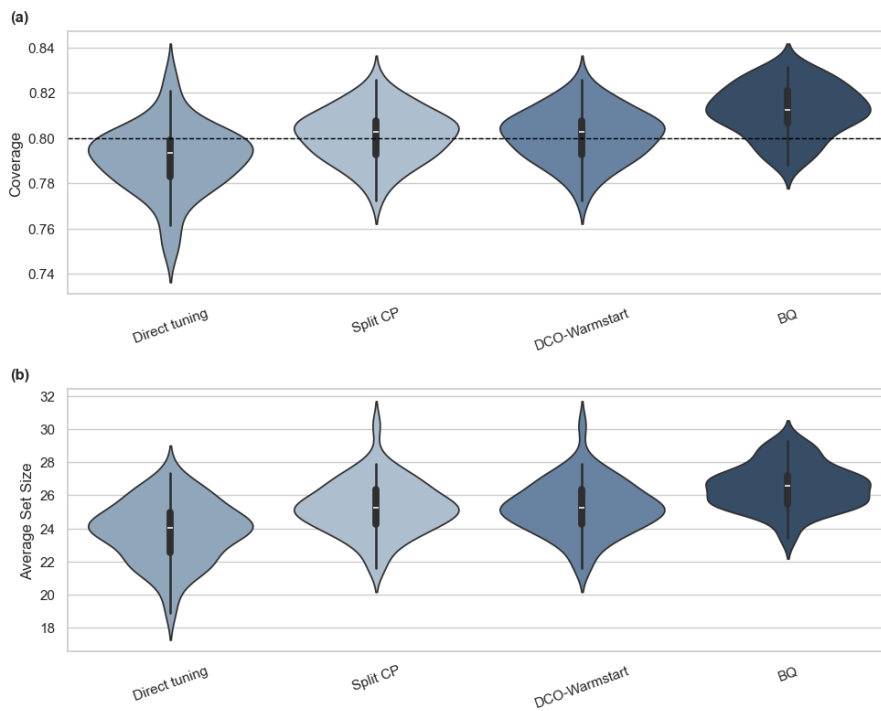


Figure 4: Distribution of test coverage (a) and prediction set size (b) on ImageNet-A across 50 random splits. The dotted line marks the target $1 - \alpha = 0.8$. DCO-Warmstart concentrates around the target with a tighter set-size distribution than BQ.

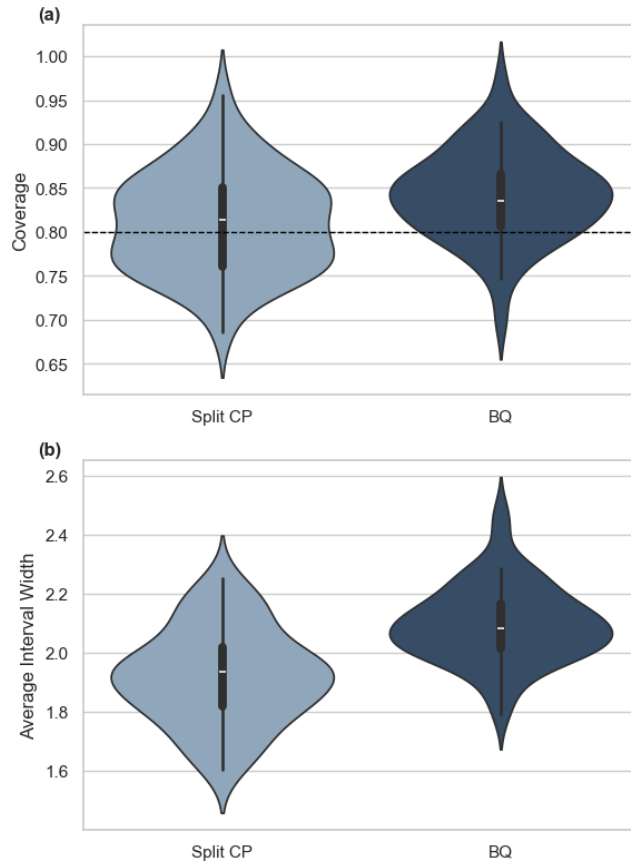


Figure 5: Coverage (a) and average interval width (b) for Split CP and BQ on the Diabetes dataset. BQ achieves higher coverage but produces wider intervals, reflecting the conservative bias of coupled threshold selection and calibration.

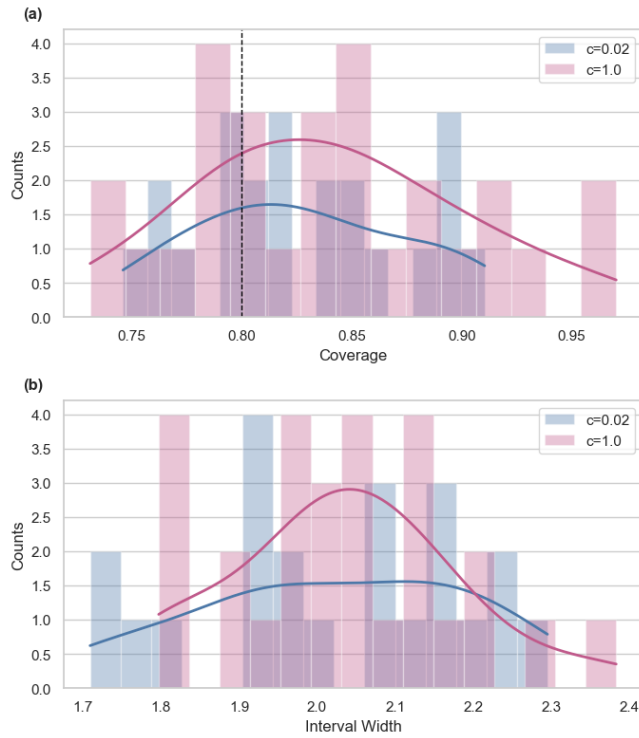


Figure 6: Coverage (a) and average interval width (b) under prior scales $c = 1.0$ and $c = 0.02$ on the Diabetes dataset across 50 splits ($1 - \alpha = 0.8$). Conformal recalibration on D_{cal} absorbs the effect of prior misspecification.